Aerodynamic Feasibility Study on Highly Distributed Lift Configurations

Andrew Truszkowski[1], Michael Mongin[1], and Aaron Altman[2]
University of Dayton, Dayton, Ohio, 45469-0238

Abstract

Preliminary experimental results showed that a highly distributed lift system (200 mini-wings) generated approximately 45% of the lift of the conventional mono-wing of equal wing area and equivalent aspect ratio. This performance was shockingly good given the penalty associated with the subscale Reynolds numbers under consideration. Hence, improvement in aerodynamic efficiency of the distributed lift configuration would be expected when scaled up to a General Aviation aircraft class scale. Taken in combination with the potential dramatic savings in wing weight, these preliminary results were considered sufficient justification to examine the concept more deeply. This paper will include the promising results of a parametric study performed using a Vortex Lattice Technique and compares those numerical results to experimental results. The results continue to suggest the possibility that the distributed lift configuration may have a practical niche when operational constraints are taken into consideration with some multi-wing configurations obtaining upwards of 60% of the lift of the equivalent mono-wing configuration.

I. Introduction

The goal of this research is to evaluate the performance potential of aircraft with massively distributed lift as achieved through multiple miniature wings when compared to the performance of the conventional standard monoplane wing. In spite of the inherent skepticism enveloping this proposed concept, there are a number of compelling reasons why this particular approach could be successful:

- Conventionally configured aircraft wings are often the heaviest components of the airplane structure.
- They are costly and difficult to manufacture, transport, and install on aircraft due to their sheer size and complexity.
- At airport terminals, much of the space airplanes occupy is a direct function of their large wingspans. Since aerodynamic lift is a strong function of the wing planform surface area, the size of the wing planform is determined based on the amount of lift desired (or weight to offset) with wing aspect ratios falling within a narrow band for a given category and class of airplane.
- These alternative [highly distributed] mini wings can be easily and inexpensively mass produced.
- They can be produced with higher effective aspect ratios than the monoplane wing.
- They can be manufactured to be considerably lighter. [1]
- Maneuverability with the mini-wings would be improved due to reduced inertia [outboard mass] and additional control from having control surfaces distributed across numerous miniature wings.
- Damage tolerance would also be improved as an airplane could afford to lose many mini wings before suffering large losses in lift.
- The wake shed from the aircraft would be an order of magnitude more compact reducing separation distances between aircraft in the vicinity of congested airports.

Theoretically (Reynolds scaling aside), if the fuselage body boundary layer is thin relative to the wingspan and the mini-wings can be spaced sufficient distances apart to minimize wing-wing interactions, the amount of lift produced by the mono-wing of an aircraft should remain the same if that mono-wing area was divided into many smaller wings placed along the fuselage. The spacing between these mini-wings would need to respect existing heuristics on vertical and horizontal spacing.

The present study was broken down into numerical and experimental phases. The first phase of this research was the numerical investigation. The objective of this portion of the study was to perform an initial potential flow, lifting surface interaction investigation on a panoply of distributed lift configurations to determine whether any synergistic multiple lifting surface interactions can be identified. Parametric variation was performed on the number surfaces, their relative proximity (stagger and gap), the number of rows and columns of miniature wings, and their

[1]Mechanical/Aerospace Engineering Student, University of Dayton, AIAA Member
[2]Aerospace Engineering Program Chair & Professor, University of Dayton, AIAA Associate Fellow

relative incidence angles. This was done through the use of two different potential flow codes. The first was the Tornado Vortex Lattice Method (Tornado VLM), a program executed through MATLAB, which allows the user to design the wing planform and run simulations under conditions set by the user. In addition, subsequent computations were performed in open Vehicle Sketch Pad's (openVSP) Aero prediction code (VSPAERO). Based on the results of these simulations, a series of the most successful designs would be identified and physically produced for use in the experimental phase.

The next phase was performed in the University of Dayton Low-Speed Wind Tunnel (UD-LSWT), which was used to measure the lift and drag characteristics of a number of distributed lift configurations. These configurations will be described in further detail in a subsequent section. These results were compared with their associated simulations in Tornado and VSPAERO in order to validate the application of these potential flow codes in terms of lift and [inviscid] drag. The results for the aerodynamic efficiencies were used to synthesize the aerodynamic inputs into the air vehicle conceptual sizing process to determine any relative advantages or disadvantages that may exist on an overall systems level. Aerodynamic penalties due to multiple lifting surface interactions will be balanced against relative weight savings (while ignoring cost savings for the moment) to arrive at an overall comparative performance between a distributed lift configuration and the baseline conventional monoplane. Preliminary experimental investigation showed that even at relatively low distributed wing Reynolds numbers (O[10,000]) losses due to fuselage boundary layer proximity were astonishingly a substantial amount less than expected. The preliminary result revealed that this approach was more viable than most aerodynamicists would imagine.

II. Previous Research

Previous studies were leveraged to provide context for the present research [2]. One study compared the effects of gap (vertical spacing between wings) and stagger (horizontal spacing between wings) on lift. In terms of gap, the smaller the gap, the smaller the downwash angle coming off the trailing edge of the wing. A smaller downwash angle implies less lift. Figure 2.1, below, provides an example.

Figure 2.1: Effect of Gap on Lift (half and one-chord gaps shown)

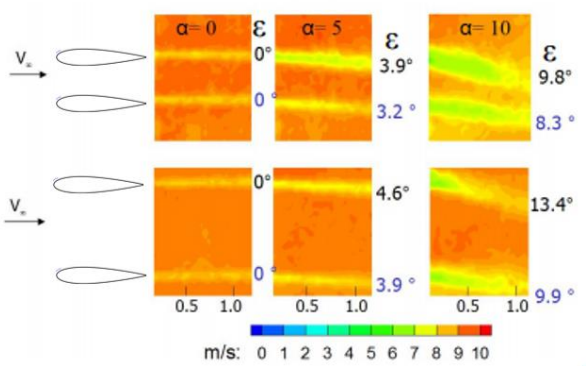

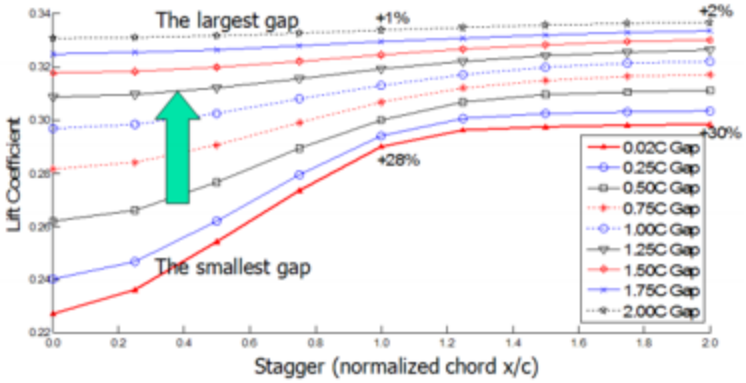

Figure 2.2: Effects of Stagger and Gap on Lift

The two comparisons depicted above in Figure 2.1 show two wings with a 0.5 chord length gap and a 1.0 chord length gap respectively. Clearly, the 1.0 chord length gap shows larger downwash angles on both of the wings, with the top wing generating the most lift in both cases. The present study did not explicitly study gap, the focus was on stagger first. A continuation of this project will incorporate gap into the wing designs as well as stagger.

Stagger was the main focus throughout the present study although gap was also investigated and reported here. In the previous study, it was also determined that the coefficient of lift decreased as the stagger decreased when the stagger was less than 1.0 chord length. An interesting conclusion from that study, however, was that beyond a stagger of about 1.2 chord lengths, the amount of lift gained as stagger increases is negligible, the lift tapers off at a certain value and the lift is no longer significantly affected by the stagger.

Figure 2.2 shows the results from previously published simulations. These results informed rational starting points for gap and stagger necessary to minimize lifting surface interactions. This valuable information was applied to the studies described in the upcoming sections.

III. Experimental and Numerical Background

A. Experimental Setup

The experimental investigation was conducted at the University of Dayton Low-Speed Wind Tunnel (UD-LSWT). The UD-LSWT has a 16:1 contraction ratio, 6 anti-turbulence screens and 4 interchangeable 76.2 cm x 76.2 cm x 243.8 cm (30” x 30” x 96”) test sections. The test section is convertible from a closed jet configuration to an open jet configuration with the freestream range of 6.7 m/s (20 m/s) to 40 m/s (140 ft/s) at a freestream turbulence intensity below 0.1% measured by hot-wire anemometer. The tunnel can also vary the freestream velocity profile at up to 5 Hz and over 50% velocity amplitude using a downstream shuttering system.

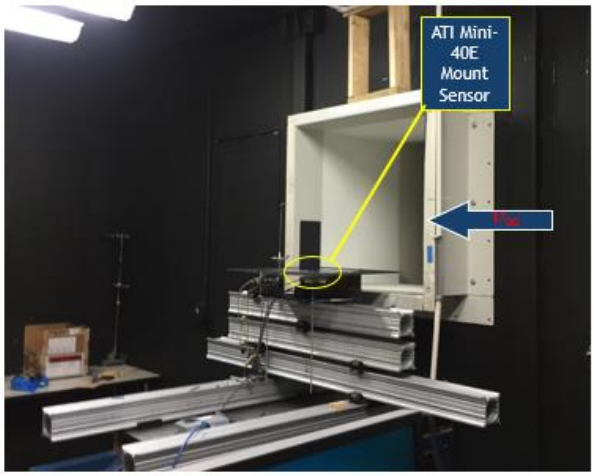

Figure 3.1: University of Dayton Low-Speed Wind Tunnel

The experiments were performed in the open jet configuration where an inlet of 76.2 cm x 76.2 cm opens to a pressure sealed plenum. Figure 3.1 shows the experimental setup. The effective length of the test section in the open jet configuration is 182 cm. A 137 cm x 137 cm collector collects the expanded air on its return to the diffuser. The velocity variation for a given RPM of the wind tunnel fan is found using a Pitot tube connected to an Omega differential pressure transducer (Range: 0 – 6.9 kPa).

ATI Industrial Automation Mini-40 and Gamma sensors were used to measure the normal (N) and axial (A) forces. The Mini-40 was used until one of the gauges stopped operating consistently. Subsequently the ATI Gamma sensor was used for the remaining tests. Lift and drag forces could be calculated from the normal and axial forces using the following equations below.

$$L = N\cos\alpha - A\sin\alpha \qquad (1)$$

$$D = N\sin\alpha + A\cos\alpha \qquad (2)$$

The specifications for the Mini – 40 sensor are as follows: the normal and axial forces were measured using the X and Y axis of the sensor with magnitude ranges of 40 N and a resolution of 1/100 N, while the torque ranges of the X and Y axes were 2 Nm with resolutions of 1/4000 Nm. The sampling rate during data acquisition from the Mini-

40 was 100 Hz. The specifications for the Gamma sensor are as follows: the normal and axial force were measured using the X and Y axis of the sensor with magnitude ranges of 65 N and a resolution of 1/80 N, while the torque ranges of the X and Y axes were 5 Nm with resolutions of 1/1333 Nm. The sampling rate during data acquisition from the Gamma sensor was 100 Hz. Wind-off tare values were taken before and after each test, and then the normal and axial force readings were adjusted for any drift that may have occurred.

B. Numerical Investigation

The first part of the numerical investigation was performed in Tornado VLM through MATLAB, a program used for linear aerodynamic wing design applications. This program allows the user to design any desired geometry; sweep, dihedral, twist, taper, trailing edge control surfaces, and airfoils are all able to be selected by the user. The user is able to easily visualize the planform through the two and three dimensional views rendered by the program, shown below.

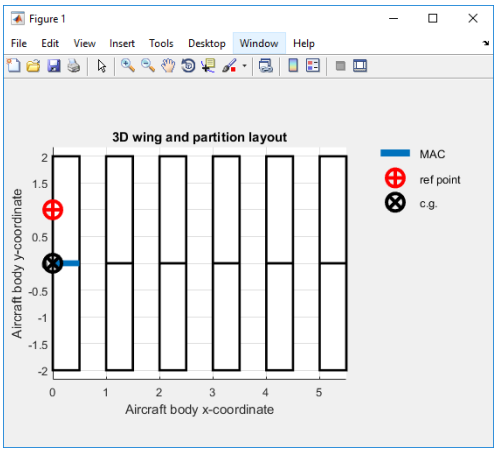

Figure 3.2 2D 6-Wing Planform Cascade in Tornado

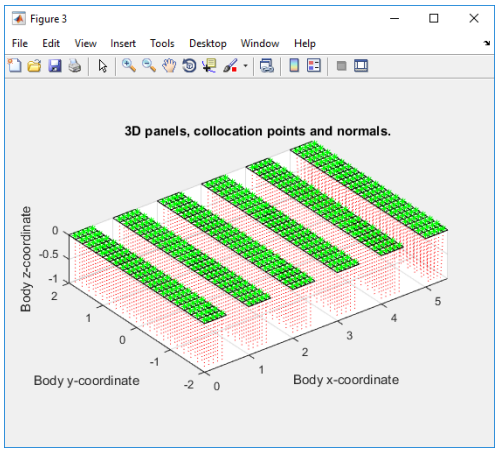

Figure 3.3: 3D 6-Wing Planform Cascade in Tornado

The program determines aerodynamic coefficients and stability derivatives. An example plot output by the program is pictured below, which shows the lift coefficient plotted against the drag coefficient, angle of attack, and pitching moment coefficient.

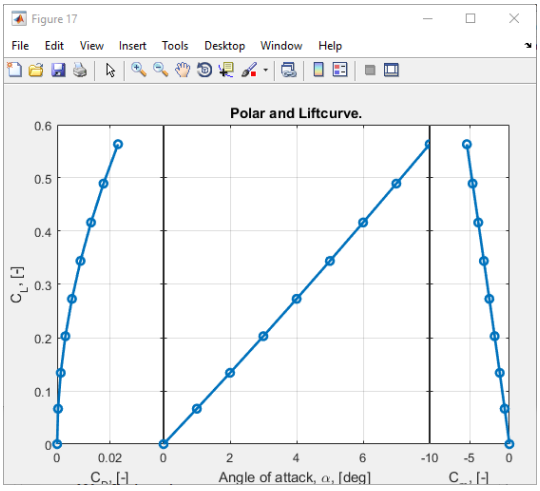

Figure 3.4: Plots Comparing Lift Coefficient to Drag Coefficient, Angle of Attack, and Pitching Moment Coefficient

VSPAERO was the second vortex method used to study the effects of lift and [inviscid] drag resulting from variations in gap, stagger, span and relative mini-wing angle of attack. This tool is an extension of the openVSP software which was released for public use by NASA in 2012. The software is centered on air vehicle design and

allows for parameterization of a wide range of design inputs. This made application of openVSP to this project natural due to its versatility in modifying geometry. As seen in Figure 3.5 and Figure 3.6, the interface for modifying wing location of the set was well designed and made changing the locations straightforward. The vortex lattice method code included with openVSP, VSPAERO, made batch processing of each wing set evident as well. VSPAERO allows the user to specify the angle of attack, angle of sideslip, and Mach number ranges for a specific geometry test set in the flow conditions input section of the dialog box. It also allows manual control of the wing area, chord, and span used for the Vortex Lattice Method (VLM) calculations. This manual control is important for these studies as many VLM codes don't use the area from the system of wings as a reference area and assume a single wing area as the Sref. In addition the process to read and process the output file from VSPAERO is effortless. The user is provided with a document in a comma separated value format that includes coefficient of lift, coefficient of induced drag, coefficient of parasitic drag, and lift over drag for each parameter specified in the flow condition input section. This format is simple to parse in Microsoft Excel and affords a rapid turnaround executing a test and combining the results next to data from multiple sources for subsequent plotting. The VSP environment enabled the discovery of relationships as a function of each parameter change made and helped in deciding which ones to investigate further through experimental study.

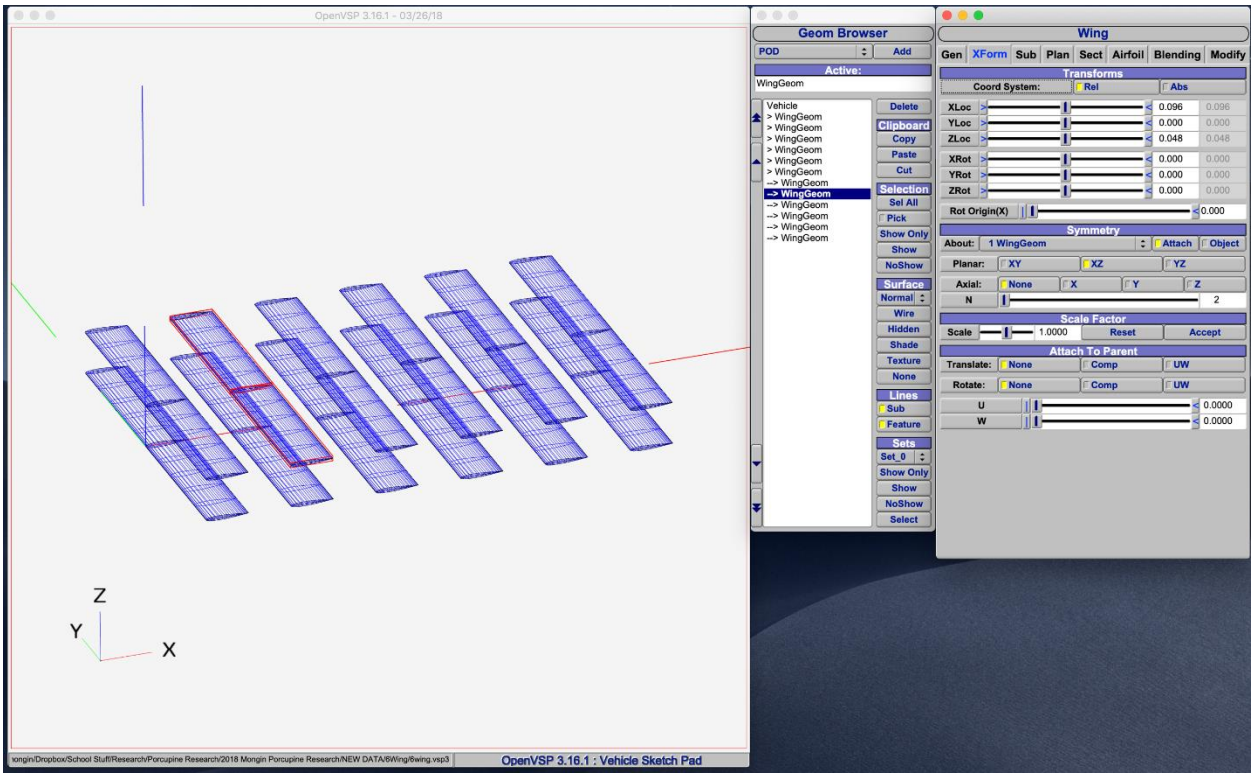

Figure 3.5: Shows the OpenVSP Rendering screen as well as the input dialog box interface for a 12-wing, 1 chord gap, 1 chord stagger case.

IV. Experimental and Computational Investigation

Testing was first performed using the two aforementioned numerical methods, then the experimental investigation was performed in the UD-LSWT as informed by the numerical results. One of the goals was to verify the accuracy of the potential flow method's predictions. The idea was thus to test a configuration/design in vortex codes, then 3D print a model of that exact layout and planform and to subsequently test it in the wind tunnel and compare the results. Initially, only configurations that were thought to be practical were considered numerically. A test matrix for the first experiment is shown in Table 4.1 below.

Later potential flow studies mostly employing VSPAERO investigated the outer bounds of the practical parameter space to determine the functional behavior related to specific parametric variations. The Gap and Stagger study test matrix can be seen in Table 4.2. The Downstream Angle of Attack variation study on configurations with no Gap can be seen in Table 4.3. Finally a variable Span and Stagger study was performed and the details behind it

can be seen in Table 4.4. It is worth noting that in testing all of the variations in Tables 4.2 – 4.4 the number of wings was fixed at 4 and the aspect ratio of all wings was 8 (semi-span AR 4).

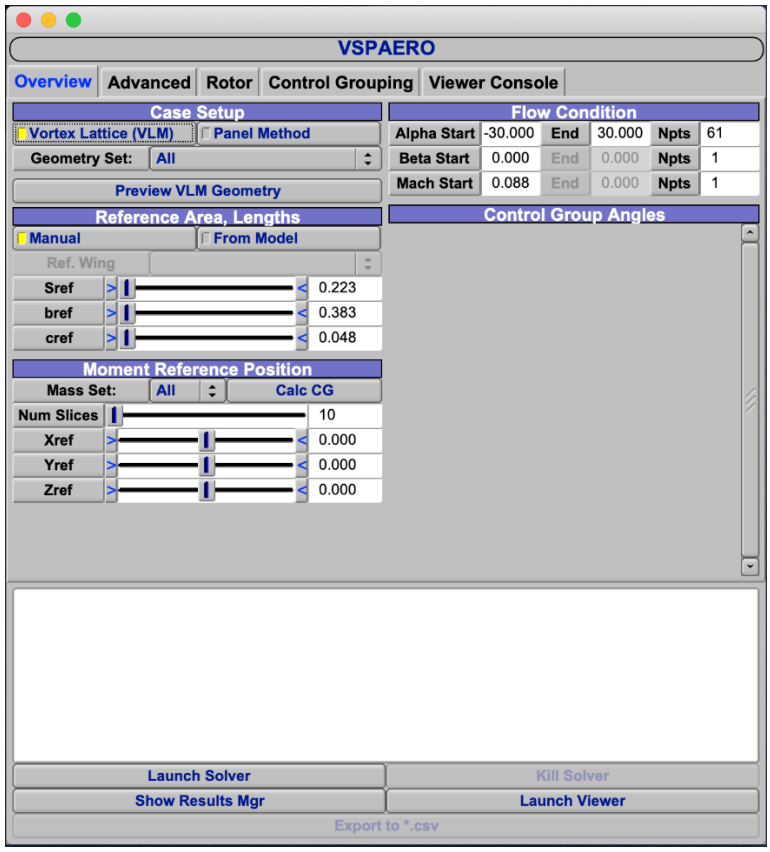

Figure 3.6: Shows the Overview tab of the input dialog box in VSPAERO and some of the variables that can be input and controlled from here.

Table 4.1: Initial Test Matrix

Method	Number of Wings (of Semispan AR 4)	Gap	Reynolds Number	Angle of Attack	Number of Trials
Tornado VLM	6	0.85c	19,325	0 to 14 deg	1
			28,988		
	3	1.7c	19,325		
			28,988		
UD Low Speed Wind Tunnel	6	0.85c	19,325		
			28,988		
	3	1.7c	19,325		
			28,988		

A. Computational Testing – Sensitivity on the Number of Wings

A taper ratio of 1 was used universally, along with a sweep angle of 0 degrees resulting in a rectangular planform for all configurations. By reducing the problem to its simplest form, it was believed that the most salient underlying physics would be identified more expediently. Symmetric airfoils (NACA 0012, to the extent that they could be reliably printed at these scales) were used throughout all wing profiles as well. For simplicity and ensuring that compressibility would not significantly affect the results the assumed constant flight conditions that each design was executed under consisted of an altitude of 4000 m and a speed of 80 m/s.

For the first part of this numerical study performed before the calculations performed for the test matrix in Table 4.1, the aspect ratios were varied between 8 and 16. Each mini-wing had a span of 2 m (for a total span of 4 m) with a chord of 0.5 m for an aspect ratio of 8 and a surface area of 2 m^2 for each mini-wing. Next, an aspect ratio of 16 was tested where the span was 5.665 m and the chord length was 0.353 m, which maintained the wing reference planform surface area of 2 m^2. The stagger between wings was varied from a half chord length, one chord length, two chord lengths, and five chord lengths. The lift curve slope (change in lift coefficient vs change in angle of attack) was calculated for each design and can be seen in Figure 4.1 below.

Table 4.2: Numerical Test Matrix for Gap and Stagger Study

Gap (in Chords)	Stagger (in Chords)	Angle of Attack (degrees)	Number of Wings
1	0, 10, 20, 40, 75	0 to 15	4
2	0, 10, 20, 40, 75	0 to 15	4
4	0, 10, 20, 40, 75	0 to 15	4
10	0, 10, 20, 40, 75	0 to 15	4
20	0, 10, 20, 40, 75	0 to 15	4
50	0, 10, 20, 40, 75	0 to 15	4

Table 4.3: Numerical Test Matrix for Downstream Angle of Attack Study on 4 Wing Configurations with No Gap

Change in Angle of Attack Downstream	Stagger (in Chords)	Angle of Attack (degrees)	Number of Wings
0	1, 0.5, 0.25	0 to 15	4
1	1, 0.5, 0.25	0 to 15	4
2	1, 0.5, 0.25	0 to 15	4
3	1, 0.5, 0.25	-5 to 10	4
4	1, 0.5, 0.25	-8 to 8	4
5	1, 0.5, 0.25	-8 to 8	4
6	1, 0.5, 0.25	-8 to 8	4
15	1, 0.5, 0.25	-14 to -30	4

Table 4.4: Numerical Test Matrix for Variable Span and Stagger Study

Span Increase Downstream (in Chords)	Stagger (in Chords)	Angle of Attack (degrees)	Number of Wings
1	2, 7, 14	0 to 15	4
1.25	2, 7, 14	0 to 15	4
1.66	2, 7, 14	0 to 15	4

The lift lost as the number of wings is increased up to about 15 wings is certainly significant, but the plot shows that beyond that, the differences in lift start to become very small. As expected, the higher aspect ratio and larger stagger configurations taper off at a slightly higher lift curve slope. Part of this observation is that in increase in stagger of 1.5 chord lengths is essentially equivalent to doubling the aspect ratio in terms of lift efficiency. Most importantly, though is the observation that whether you have 15 wings or 50 wings, there won't be a substantial difference in terms of lift between those configurations. More wings could result in greater control, thus it is noteworthy for future study that adding more than fifteen wings has few significant drawbacks.

Next, the slope of the lift coefficient squared (C_L) vs drag coefficient (C_D) was plotted in order to see if they behave similarly. The drag polar plots the lift coefficient against the drag coefficient, but since the line of that graph is quadratic, it is hard to numerically compare results against themselves. However, when the lift coefficient term is squared, that line becomes essentially linear, which allowed the slope of that line to be taken so that different configurations could be compared together in a similar fashion to those in Figure 4.1. Figure 4.2 below shows how the drag polar changes when the lift coefficient term is squared.

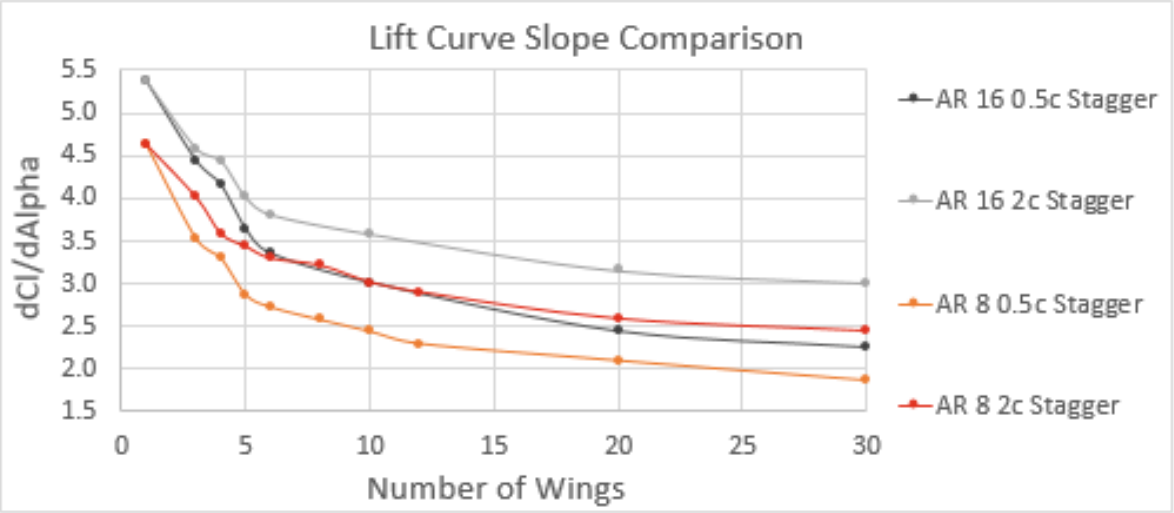

Figure 4.1: Lift curve slope result show a rapid dropoff in lift performance for the first 10 to 15 wings and a subsequent leveling off of the lift penalties beyond that. In increase in stagger of 1.5 chords equals the impact on lift efficiency of doubling the aspect ratio.

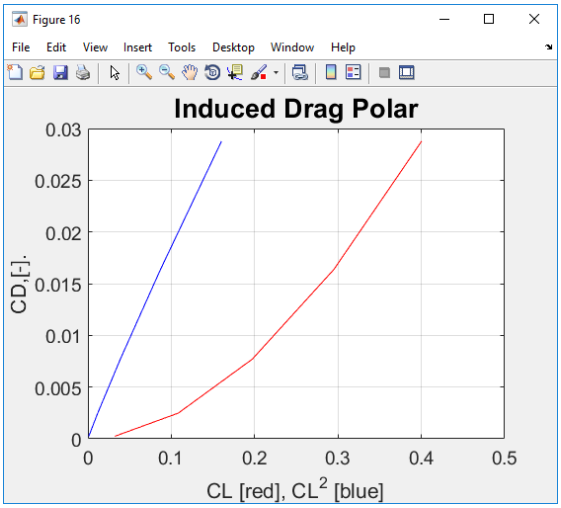

Figure 4.2: Converting the Drag Polar to Linear

All the results obtained from the Tornado program were converted so that a linear relationship was preserved throughout these tests. Select results of this portion of the research can be viewed below in Figure 4.3.

Similar to the lift curve slope comparisons, these results taper off at a certain number of wings as well. Again, the higher aspect ratio and stagger configurations asymptote to a higher value due to the reduced influence of wingtip vortices. The results here are consistent with the lift curve slope results. When adding the number of wings beyond about 25 wings, there is not a significant amount of additional lift lost.

In addition, the lift curve slope was shown as a percentage of the Helmbold lift curve slope value. The Helmbold equation gives the ideal aspect ratio corrected lift curve slope (in this range of aspect ratio), which helped accurately compare the results across the different aspect ratios. The Helmbold equation is shown in Eq. (3) below as:

$$C_{L\alpha} = \frac{\pi AR}{\left[1+\sqrt{1+\left(\frac{AR}{2}\right)^2}\right]} \quad (3)$$

Since only two aspect ratios were used initially, 8 and 16, these Helmbold-corrected lift curve slopes were substituted into Eq. (3) and are shown in Table 4.5 below.

Table 4.5: Helmbold Lift Curve Slope Values

AR	Helmbold dCl/dAlpha
8	4.906/rad
16	5.547/rad

Based off of these values, cross plots were generated in Figure 4.4 (below) that showed the lift curve slope values as a percentage of the values in the table above.

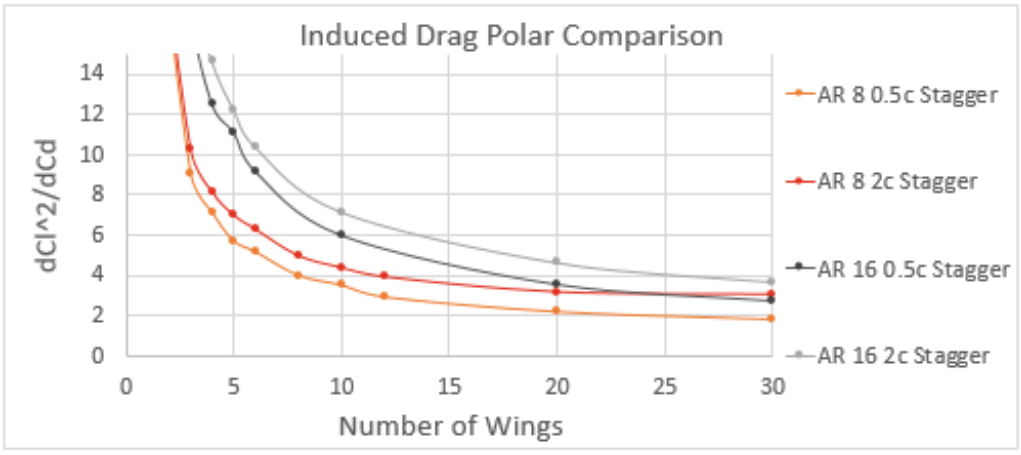

Figure 4.3: Induced Drag Polar Comparison

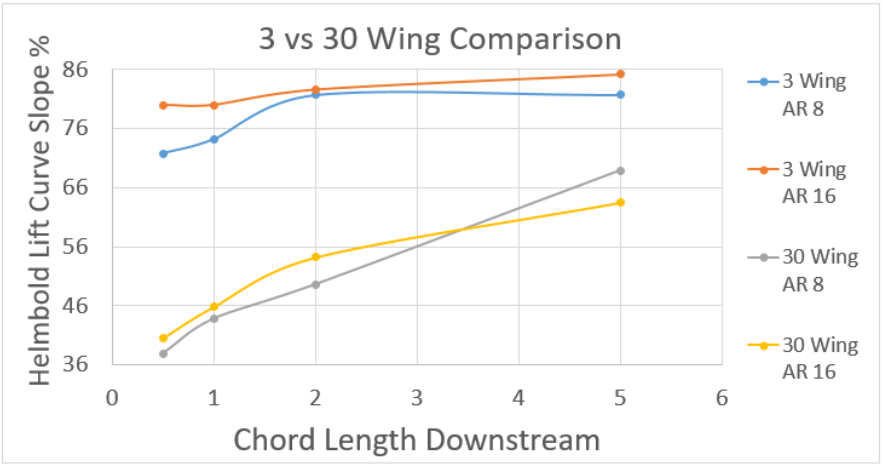

Figure 4.4: A 30 Wing Configuration shows that a 5 chord-length spacing 30 mini-wing configuration will begin to approach the performance of the 3-Wing configuration when compared along the common Helmbold lift slope baseline.

Figure 4.4 shows a number of different configurations that consisted of three and thirty wings where the aspect ratio and stagger (in terms of chord length) were varied. The aspect ratio 16 configurations were all more efficient in the 3 wing tests. However, when the number of wings increased to 30, the results showed that the aspect ratio 8 configurations actually started to be more efficient when the stagger was large enough. It is useful to know for future testing because it raises the question whether adding an even greater number of wings, perhaps the lower aspect ratio designs will be more efficient at an even smaller stagger. This would keep the moment of inertia even lower and allow for even more increased maneuverability.

The testing from the Tornado VLM program was valuable, but the inviscid flow assumptions presented some lingering questions on how accurately the program predicts lift at these Reynolds numbers, so the upcoming wind tunnel results hoped to provide more confidence in the results of the potential flow codes.

B. Computational Testing – Sensitivity on Stagger

One sensitivity was performed to determine the isolated effects of stagger across a variety of multi-wing configurations. The results shown here are considered to be representative of the results generated, however the results shown here comprise only a subset of those studied. The behavior seen in this sensitivity is similar to that observed across numerous other sensitivities and thus these results were considered one of the most lucid and concise manners in which to demonstrate the most salient features.

Figure 4.5 elucidates the behavior of the lift curve slope as a function of stagger for a 4-wing configuration seen in Figure 4.6. There is a rapid improvement in lift efficiency of approximately 17% in the first 20 chord lengths of downstream spacing when gap is fixed at 2 chord lengths. As stagger approaches an infinite distance, only another approximately 5% improvement can be gained beyond 20 chord lengths of stagger.

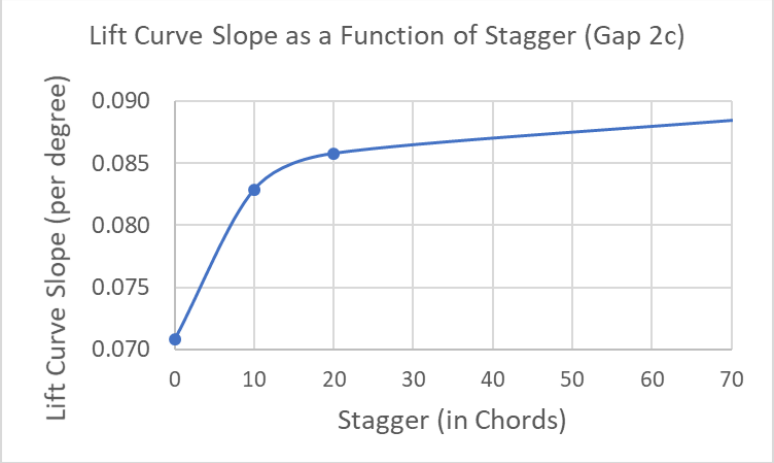

Figure 4.5: The lift efficiency plateaus beyond a 20 chord stagger in the case of the 2 chord gap.

Figure 4.6: A side view of the 2-chord gap 10 chord stagger case rendered in VSPAERO.

Figure 4.7 shows a systematic improvement in aerodynamic efficiency as a function of decreasing stagger with the maximum obtained by the mono-wing and the lowest stagger case demonstrating the worst performance. Figure 4.8 plots these maximum lift to drag ratio peaks as a function of their stagger. The performance improves rapidly from the lowest stagger case towards the mono-wing case with an approximately 9% improvement from a 75 chord stagger to the mono-wing versus an approximately 32% improvement for the no stagger case.

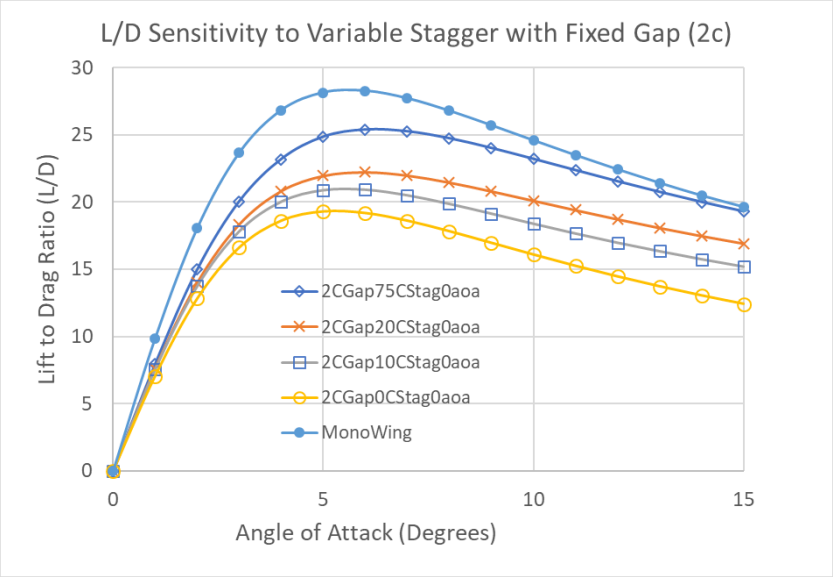

Figure 4.7: The maximum lift to drag ratio improves systematically from no stagger to the mono-wing case.

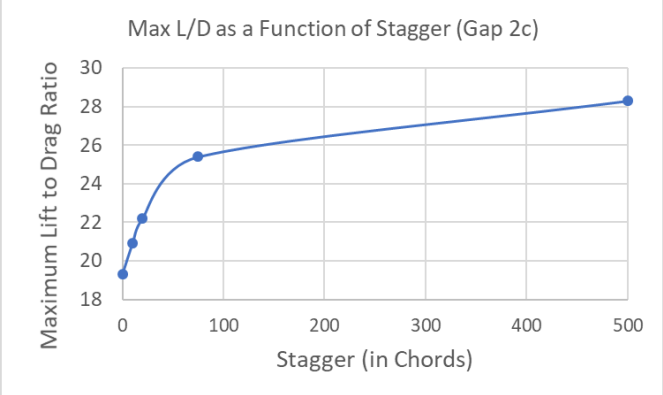

Figure 4.8: The maximum lift to drag ratio improves roughly 9% from the greatest stagger distance case to the conventional mono-wing configuration for a 2 chord gap, and approximately 32% from the no stagger to the conventional mono-wing case.

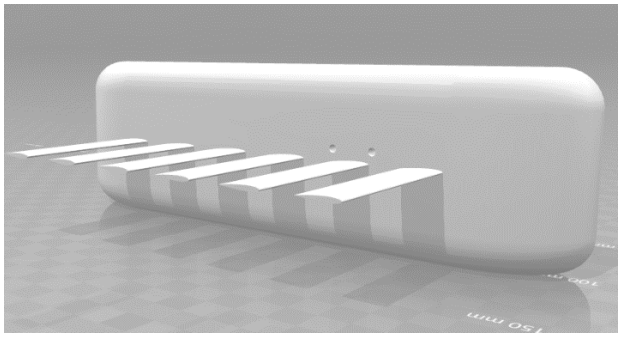

Figure 4.9: First Generation of a 6 Wing Configuration to be Tested in UD-LSWT

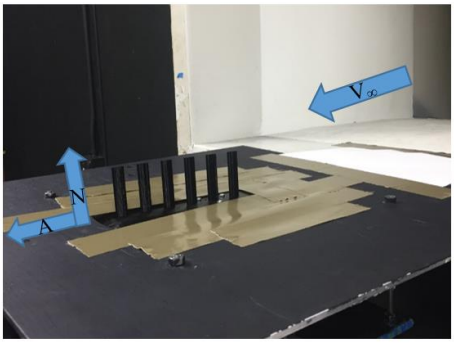

Figure 4.10: One of the 3-D Printed models in the test section

C. Experimental Testing

The first model tested in the UD-LSWT was created in SolidWorks and then 3-D printed. The model consisted of six NACA 0012 wings, each having a semi-span of 2.3 in (0.0584 m) and a chord length of 0.575 in (0.0146 m) which gave each mini-wing a semi-span AR of 4 and surface area of 1.323 in^2 (0.005116 m^2). Each of the wings were spaced out with a stagger of 85% of the chord length. Figure 4.9 shows the .stl file that was 3-D printed.

The fuselage [péniche] was below the freestream to provide the closest comparison to the numerical results which only accounts for the wings and not the fuselage of the aircraft as implemented. There will still likely be minor influence from the thin boundary layer developed on the flat plate/floorplane however this influence will only penalize the results of the distributed lift configurations as compared to the conventional mono-wing.

Figure 4.10, pictured above, shows a 6-wing model in the test section. In addition, a model of the exact same dimensions was created in Tornado VLM with the intention of testing the robustness of the inviscid assumption in application to the lifting surface interactions associated with this problem. The Reynolds numbers for the individual highly distributed wings were 19,325 (20 m/s free stream velocity) and 28,988 (30 m/s free stream velocity), and the results are shown in the graph below.

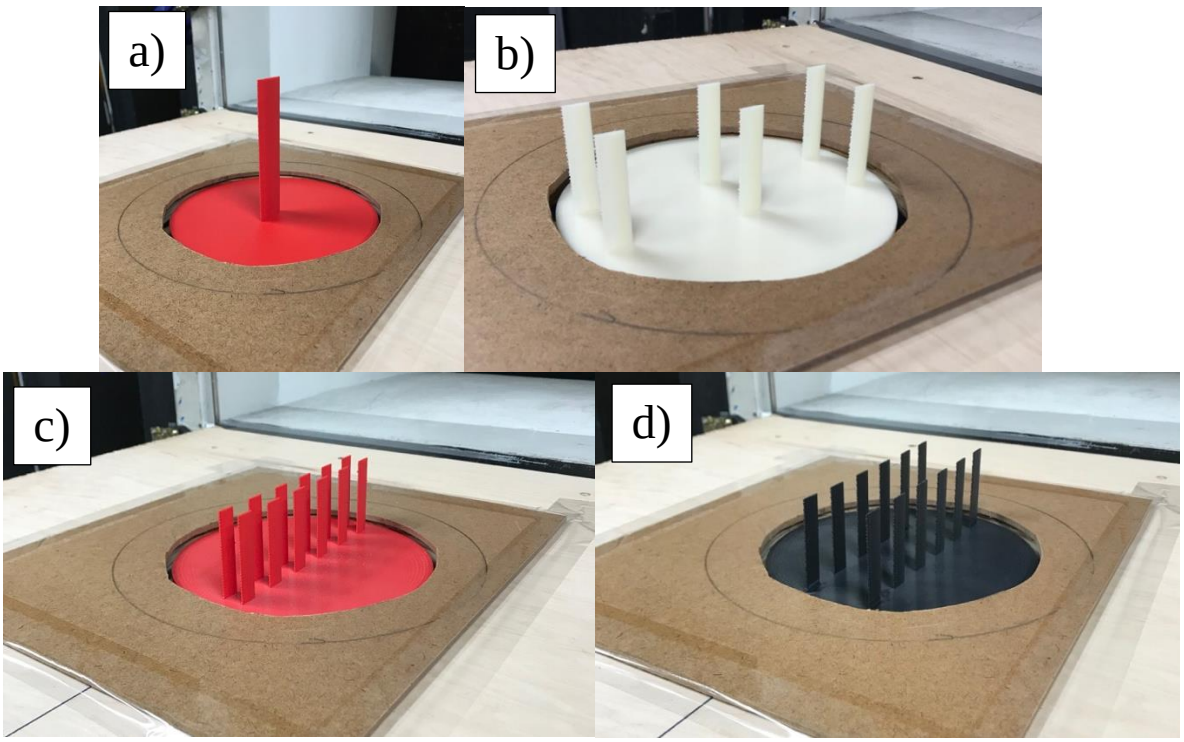

Figure 4.11: Shows four more configurations tested: a) Mono-wing, b) 6-wing – 3c Gap and 5c Stagger, c) 12-wing - 1c Gap and 1c Stagger, d) 12-wing - 3c Gap and 1c Stagger

The next generation of multi-wing models were constructed via 3D printing as well and incorporated a baseplate with attached wings design. Four models were constructed, a mono-wing (Figure 4.11a), a multi-wing of 3 chord gap and 5 chord stagger (Figure 4.11b),a multi-wing of 1 chord gap and 1 chord stagger (Figure 4.11c), and a multi-wing of 3 chord gap and 1 chord stagger (Figure 4.11d). Table 4.6 lists the test conditions for these models. The mini-wings were the same dimensions as the previous model, 0.0146 m chord and 0.0584 m semi-span. The mono-wing was created at a third the area of the combined 12 wing set due to manufacturing limitations. Its chord was 0.029 m and span 0.117 m. The area of the 12 wing set was 0.0103 m^2 and the area of the mono-wing was 0.00345 m^2. A 4.5 mm thin cover was constructed out of fiberboard to prevent secondary flows from entering the gap between the rotating test model and the opening in the test stand top. Figure 4.12 shows the under-floor setup.

Table 4.6: Lists the experimental test conditions for the various models tested.

Test Model	Gap (Chords)	Stagger (Chords)	Number of Wings	Velocity (m/s)	Angle of Attack (Degrees)	Test Method
Mono-Wing	**N/A**	**N/A**	**1**	**30 and 35**	**-40 to 40**	**VLM and Wind Tunnel**
Figure 4.11c	**1**	**1**	**12**	**30 and 35**	**-40 to 40**	**VLM and Wind Tunnel**
Figure 4.11d	**3**	**1**	**12**	**30 and 35**	**-40 to 40**	**VLM and Wind Tunnel**
Figure 4.11b	**3**	**5**	**6**	**30 and 35**	**-40 to 40**	**VLM and Wind Tunnel**

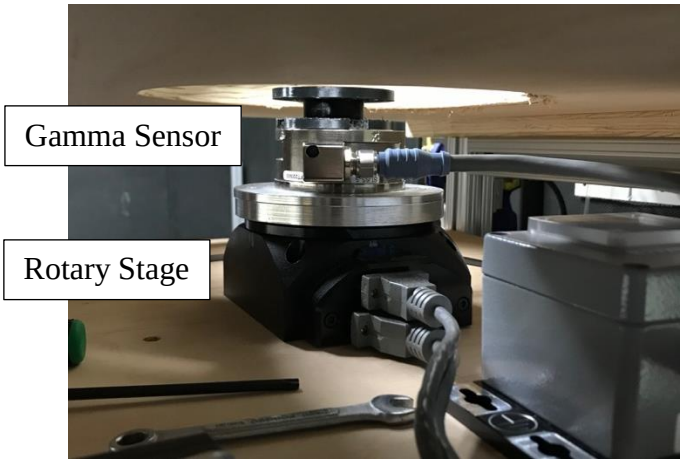

Figure 4.12: The underfloor test setup including the ATI Gamma Sensor and the rotary stage for setting angle of attack.

The Tornado VLM program ran a simulation at 30 m/s for the model pictured in Figure 4.10, and then that result was plotted alongside the two experimental tests in addition to the Tornado monoplane results where all of the configurations had the same aspect ratio and surface area. Of course, the monoplane simply did not include the distributed lift interaction. The experimental and Tornado lift results for the distributed lift configurations (Figure 4.13) were strikingly similar as all three plots showed minimal differences. As expected, the monoplane had a significantly higher lift curve slope, but that must be taken into context against the benefits that the distributed lift configurations could potentially have.

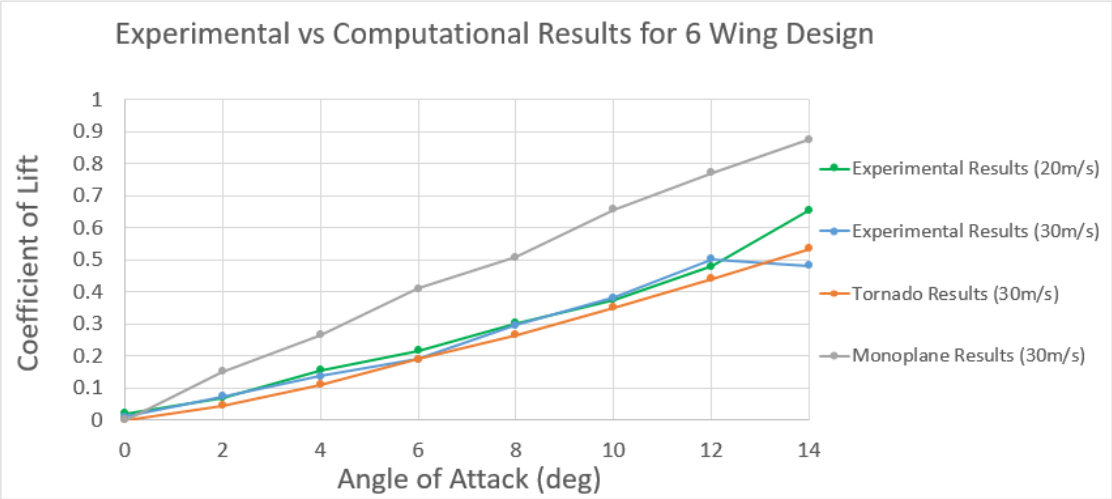

Figure 4.13: Shows good agreement between experimental and potential flow code results in lift.

The multi-wings exhibit behavior approximating that of low aspect ratio wings in Figure 4.14. None of the multi-wings appear to experience a complete stall prior to approximately 35 degrees at which point they achieve almost the same maximum lift as the mono-wing (albeit at much higher drag). Additionally, depending upon the spacing between the multi-wings the lift achieved is considerably higher than expected with the better multi-wing case achieving almost 70% of the lift curve slope of the mono-wing.

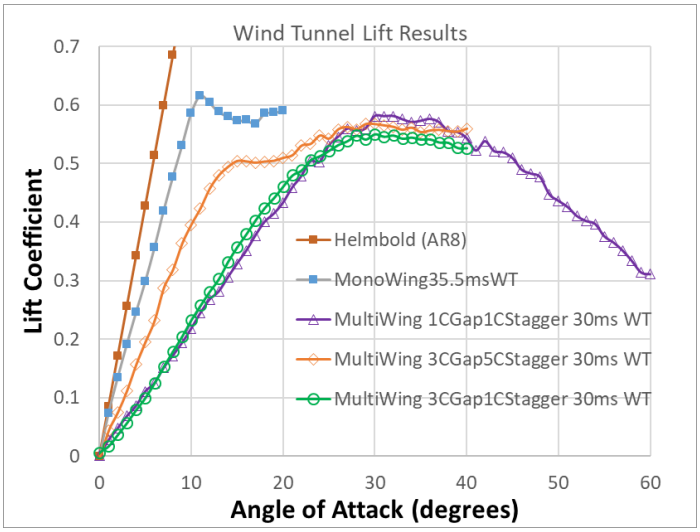

Figure 4.14: Shows that the multi-wing configurations stall at extremely high angles of attack and that the 3 chord gap 5 chord stagger case performs relatively well compared to the mono-wing.

A limited subset of lift curve slopes resulting from VSPAERO are compared to experimental results in Figure 4.15. Although the absolute values obtained for the slopes are not in very good agreement, the general trends are relatively close. Given the relatively low Reynolds numbers of the multi-wing configurations, it is likely that laminar separation bubble behavior is not being modeled by the potential flow codes used.

A comparison between the VSPAERO derived drag results and the experimental results can be seen in Figure 4.16. Drag was estimated from VSPAERO by calculating the lift induced drag and adding the experimentally determined base drag. This was done to facilitate a direct comparison between the numerical and experimental results. As would be expected the drag for the multi-wing cases is higher than that generated from the VSPAERO code.

Figure 4.17 shows comparative experimental results for the relative aerodynamic efficiencies of several configurations. There is an approximately 25% difference between the best and worst performing multi-wing

configurations. The best performing multi-wing configuration obtains an aerodynamic efficiency of approximately 61% of the mono-wing aerodynamic efficiency. This is a result that the authors found quite surprising.

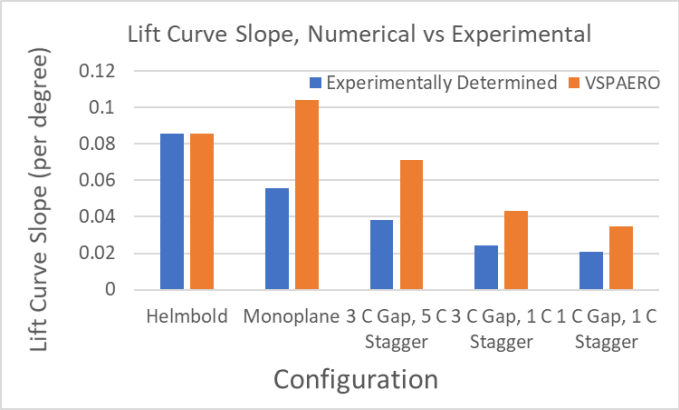

Figure 4.15: Demonstrates similar trends in predicted versus experimentally determined lift curve slope although there is a significant difference in absolute value.

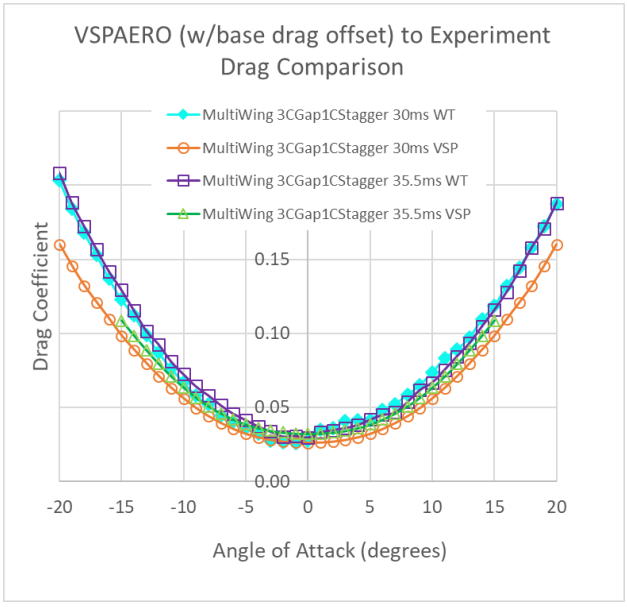

Figure 4.16: Compares a set of multi-wing VSPAERO results against wind tunnel results. The VSPAERO results have the experimentally determined base drag added to facilitate comparison.

V. Conclusion

More detailed study of the effects of induced angle of attack on wings downstream might lead to slightly more efficient results. Despite the differences seen between the numerical and experimental results some conclusions can still be made. In terms of the overall feasibility of distributed lift configurations from an exclusively aerodynamic standpoint, much less lift is generated when these mini-wings are used. However, due to the fact that these configurations would be lighter, less lift would need to be generated. These distributed lift designs would have a large number of benefits that could potentially outweigh the lift penalties ranging from increased maneuverability, improved damage tolerance, a more compact aircraft that is easier to store/park and an aircraft that needs much less room to take off and land. Therefore the authors firmly believe that based on the results presented here, the potential of practical application of these configurations warrants further study on an overall air vehicle systems-level design.

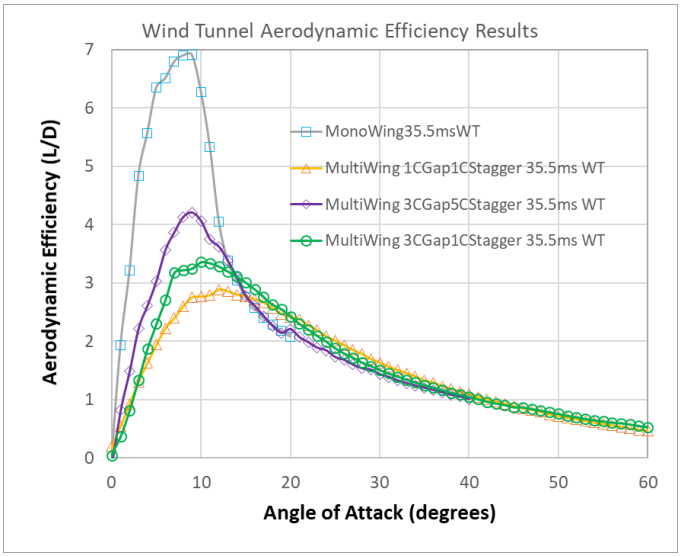

Figure 4.17: There is an approximately 25% difference between the best and worst performing multi-wing cases and the best performing multi-wing achieves roughly 61% of the mono-wing lift.

References

[1] Raymer, Daniel P. *Aircraft Design: A Conceptual Approach*, AIAA, 1992.

[2] Kang, H., Genco, N., Altman, A., *Gap and Stagger Effects on Biplanes with End Plates Part I*, AIAA 09 -1085, 47th AIAA Aerospace Sciences Meeting and Exhibit, January 2009, Orlando, Florida.